Hydrodynamic analog of particle trapping with the Talbot effect

N. Sungar[*]

Department of Physics, Cal Poly State University, San Luis Obispo, California 93407, USA

L. D. Tambasco, G. Pucci, P. J. Sáenz, and J. W. M. Bush

Department of Mathematics, Massachusetts Institute of Technology, Cambridge, Massachusetts 02139, USA

We present the results of an experimental study of the standing waves produced on the surface of a vertically shaken fluid bath just above the Faraday threshold, when a row of equally spaced pillars protrudes from the surface. When the pillar spacing is twice the Faraday wavelength, the resulting wave field is marked by images of the pillars projected at integer multiples of a fixed distance from the row. This projection effect is shown to be analogous to the well-known Talbot or self-imaging effect in optics, and a Faraday-Talbot length is defined that rationalizes the location of the images. A simple model of point sources emitting circular waves captures the observed patterns. We demonstrate that the images may serve as traps for bouncing and walking droplets.

I. INTRODUCTION

Hydrodynamics has long served as a rich source of physical analogy. Newton described corpuscles of light generating waves through the ether like stones dropped on a pond [1], while Thomas Young argued the wave nature of light by analogy with ripple tank experiments [2]. On an astrophysical scale, hydrodynamic analogs of black holes [3] and white holes [4] have been explored. In the quantum realm, both the Aharanov-Bohm [5] and Casimir effects [6] have been examined using fluid analog systems. The quantum-like features of droplets walking on a vibrating fluid bath [7,8] are a subject of growing interest [9,10].

As first reported by Faraday [11] in 1831, the free surface of a fluid bath vertically vibrated with amplitude A, frequency f, and acceleration $\Gamma(t) = \gamma \cos(2\pi f t)$ may become unstable to standing surface waves with frequency $f/2$. For a vibrational acceleration $\gamma = A(2\pi f)^2$ below the Faraday threshold γ_F, the free surface is stable. For $\gamma > \gamma_F$ the surface becomes unstable to subharmonic Faraday waves with wavelength $\lambda_F = 2\pi/k_F$ prescribed by the standard water-wave dispersion relation

$$\omega^2(k) = \left(gk + \frac{\sigma}{\rho}k^3\right)\tanh(hk), \tag{1}$$

where k is the wave number, g the gravitational acceleration, σ the surface tension, ρ the fluid density, and h the fluid depth. Faraday waves have been extensively investigated both experimentally and theoretically [12–14]. Just below the Faraday threshold $\gamma < \gamma_F$, perturbations of the surface generate Faraday waves that decay over a characteristic memory time $T_M = \lambda_F^2/[8\pi^2\nu(1 - \gamma/\gamma_F)]$, where ν is the fluid's kinematic viscosity. The Faraday system has recently been used to study hydrodynamic quantum analogs, as may arise when millimetric droplets levitating on the vibrating bath self-propel through a resonant interaction with their own wave field [7–9].

The optical Talbot effect occurs in the near field when a monochromatic wave is modulated by a spatially periodic structure [15]. The effect was discovered in 1836 by Henry Fox Talbot in his examination of the optical pattern behind an illuminated diffraction grating [16]. The supporting
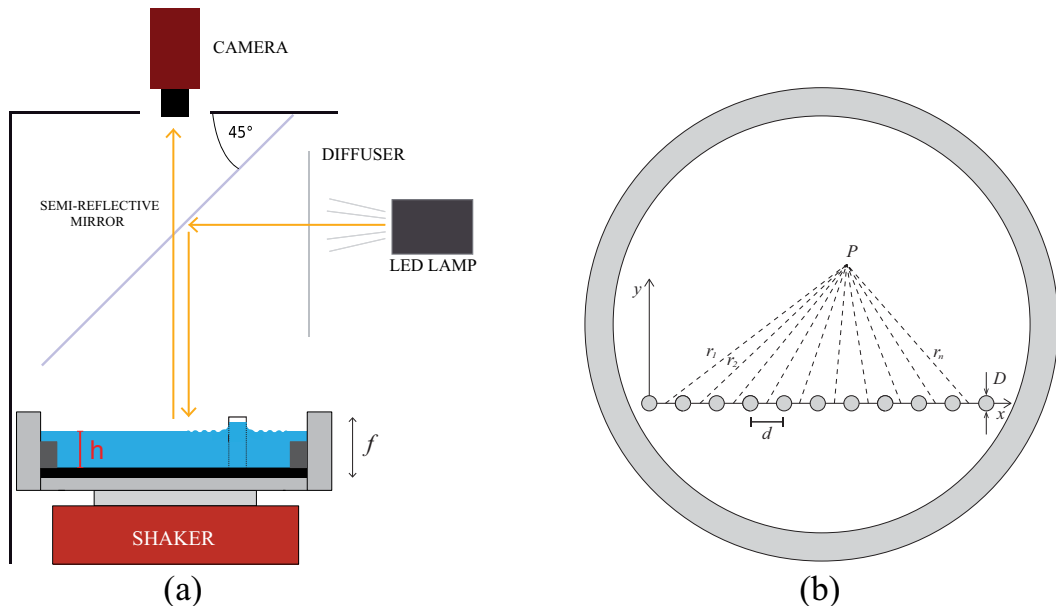
————
[*]nsungar@calpoly.edu

FIG. 1. (a) Experimental arrangement [27]. The fluid bath is shaken using an electromagnetic shaker and imaged using a CCD camera through a $45°$ semireflective mirror with diffuse illumination [12]. (b) Top view of the fluid bath shows the row of N protruding pillars of diameter D and center-to-center separation d.

theory was developed in 1881 by Lord Rayleigh, who showed that the effect results from the interference of monochromatic, coherent waves emitted from the diffraction grating [17]. In his analysis, Rayleigh expressed the optical field resulting from the interference of waves from individual slits in terms of a sum over monochromatic plane waves with wavelength λ and transverse wave-vector components $2\pi n/d$, where d is the slit spacing and $n \in \mathbb{N}_0$. He showed that, at integer multiples of a distance z_T perpendicular to the grating, the intensity distribution at the grating is reproduced. This distance, called the Talbot length, is given by

$$z_T(\lambda) = \frac{\lambda}{2\left(1 - \sqrt{1 - \left(\frac{\lambda}{d}\right)^2}\right)}. \tag{2}$$

When $\lambda \ll d$, Eq. (2) reduces to a better-known formula for the Talbot length $z_T = d^2/\lambda$. The analysis shows that, at even integer multiples of the Talbot length, self-images are spatially in phase with the grating. At odd integer multiples of the Talbot length, self-images are shifted by half the slit spacing ($d/2$), and so are referred to as shifted self-images [18].

The Talbot effect has since been extensively studied and applied in optics [19,20]. This phenomenon has also been used in a variety of applications including optical trapping of atoms [21] and particles [22], atom wave interference [23], Bose-Einstein condensates [24], plasmonics [25], and x-ray imaging [26]. We here present a hydrodynamic analog of the Talbot effect in the Faraday system, and demonstrate its ability to trap bouncing and walking droplets.

II. THE HYDRODYNAMIC TALBOT EFFECT

A. Experiment

The setup consists of a circular bath 15.8 cm in diameter that is vertically shaken and imaged from above using a diffuse light source. A schematic of the experiment is shown in Fig. 1. Silicone oil of viscosity $\nu = 20.9$ cS, density $\rho = 950$ kg/m^3, and surface tension $\sigma = 20.6$ mN/m fills the circular
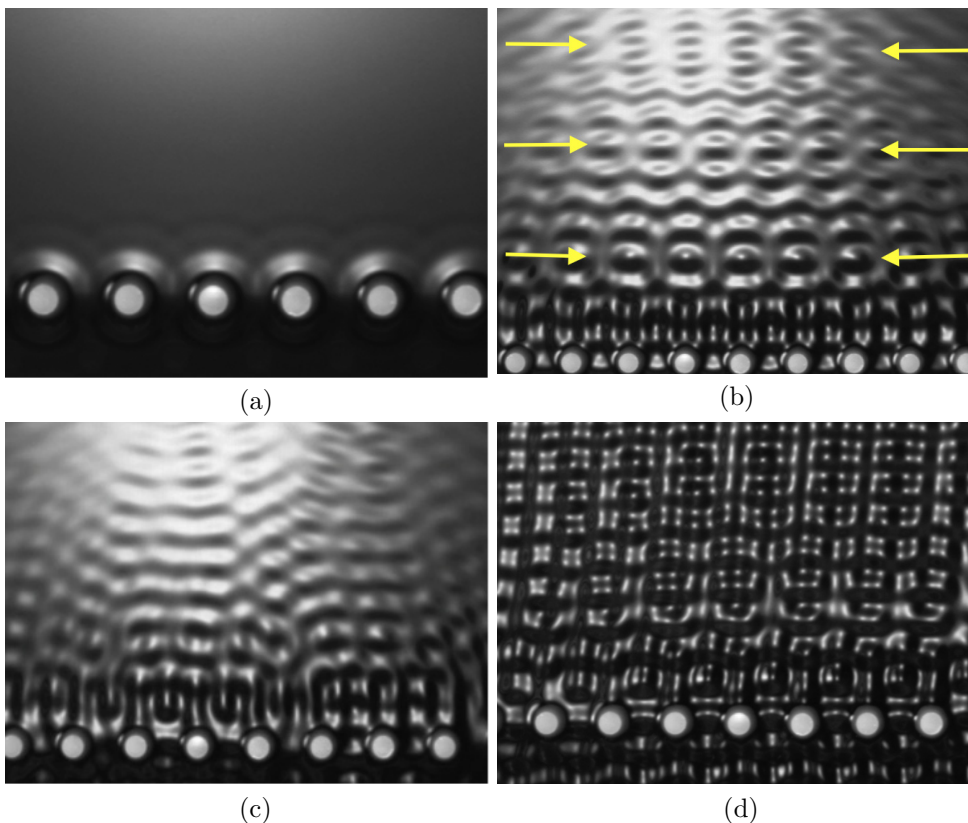
FIG. 2. The surface of the shaken fluid. Pillars with diameter $D = 3.1$ mm are spaced $d = 9.5$ mm apart from center to center. (a) $f = 80$ Hz, $\gamma = 0.99\gamma_F$. Meniscus waves are evident around the pillars. (b) $f = 80$ Hz, $\gamma = 1.007\gamma_F$. Rows of images in front of the pillars are marked with arrows. (c) $f = 70$ Hz, $\gamma = 1.007\gamma_F$. The pattern has lost its periodicity. (d) $f = 80$ Hz, $\gamma = 1.012\gamma_F$. The self-imaging pattern is lost, replaced by a checkerboard of Faraday waves.

bath to a depth of $h = 6.10 \pm 0.05$ mm. The bath is surrounded by a shallow region of depth 1.1 mm and width 12.7 mm that serves to damp the waves at the bath boundaries. A linear, periodic array of N pillars, each with diameter $D = 3.1 \pm 0.1$ mm and separated by a center-to-center distance d, protrudes from the bath to a height of 2.1 mm above the fluid surface.

The recording camera directly above the bath images the surface at a frame rate slightly higher than $f/4$ in order to reveal fast oscillations in the observed patterns. The setup is illuminated from the side by an LED lamp, and the light is redirected by a $45°$ semireflective mirror, as shown in Fig. 1. The incident light is normal to the bath, then reflects back to the camera. With this imaging technique, flat areas of the interface appear as bright regions, sloped areas as dark regions.

We report here experimental results with two different array separations of $d = 9.5$ mm and $d = 12.5$ mm with a total number of pillars $N = 14$ and $N = 11$, respectively. Arrays with larger d necessarily had a smaller number of pillars and so produced images only in the central region of the near field. Forcing frequencies in the range of 40–90 Hz were explored for each array. At every frequency investigated, the Faraday threshold γ_F was determined by decreasing γ, initially above γ_F, by decrements of $0.01g$ until Faraday waves far from the boundaries died out within 1 minute. The Faraday threshold is then set to be $0.005g$ above this acceleration.

We note that meniscus waves of the form seen in Fig. 2(a) are evident around the pillars even for $\gamma < \gamma_F$. The static menisci attached to the pillars have a characteristic height corresponding to the

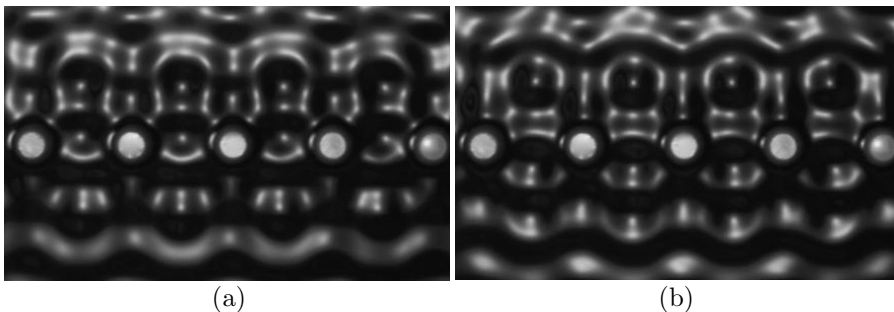(a)   (b)

FIG. 3. Video frames showing the wave field around the pillars, captured $T_F/2$ apart. The waves on either side of the pillars are temporally out of phase and the interpillar ridge sloshes back and forth in synchrony with the wave patterns.

capillary length $\sqrt{\sigma/\rho g} \approx 1.5$ mm. When the bath is shaken, the variation in g causes the menisci to oscillate, emitting waves at the driving frequency f with a wavelength $\lambda_M = 2\pi/k_M$ (of order 3 mm for the frequencies considered) prescribed by Eq. (1) that is notably different from λ_F. We note that the attenuation length of the harmonic meniscus waves can be shown to scale as $c(k_M)/(2\nu k_M^2)$, where $c(k) = d\omega/dk$ is the group velocity [28]. For the range of frequencies considered, this attenuation length is of order 2 mm, consistent with Fig. 2(a), where meniscus waves are seen to extend no further than 1 cm beyond the pillars. While meniscus waves contribute negligibly to the far field, they do modify the waves near the pillars, perturbing and coupling to the subharmonic Faraday waves that emerge for $\gamma > \gamma_F$.

In a narrow range of driving frequencies that depends on the pillar spacing, standing wave patterns that replicated the periodicity of the pillar array were apparent [see Fig. 2(b)]. Outside this frequency range, patterns did not form regular periodic structures and were distorted with defects as shown in Fig. 2(c). We note that, even at the requisite driving frequency, sharp self-images were observed only at accelerations within 0.2–1% of γ_F. At higher γ, the self-image was destroyed and a checkerboard of Faraday waves, such as those shown in Fig. 2(d), dominated the fluid surface. High speed videos of the fluid motion reveal that the oscillation frequency of the pattern of all the pillar images is the resonant subharmonic, $f/2$, indicating that the patterns result from interfering Faraday waves.

The self-imaging arises over a narrow frequency range in which the center-to-center pillar spacing corresponds to approximately twice the Faraday wavelength $d \approx 2\lambda_F$. For the array with $d = 9.5$ mm, the self-imaging is observed for $f = 78$–82 Hz, corresponding to a Faraday wavelength range of $\lambda_F \approx 4.7$ mm and meniscus wavelength $\lambda_M \approx 2.8$ mm. Similarly, for the array with $d = 12.5$ mm, self-imaging happens at 57–61 Hz, corresponding to $\lambda_F \approx 6.0$ mm and $\lambda_M \approx 3.6$ mm. In both cases, at the frequencies where self-imaging arises we observe that curved ridges form between the pillars, and slosh laterally, normal to the array direction, in phase with each other at $f/2$. Two video frames, taken half a Faraday period $T_F/2 = 1/f$ apart, are shown in Fig. 3. The patterns on opposite sides of the pillar arrays are temporally out of phase, following the phase of the sloshing interpillar ridges [29].

We attribute these sloshing interpillar ridges to the interaction of Faraday and meniscus waves in the vicinity of the pillars. For an individual pillar at the onset of instability, $\gamma \gtrsim \gamma_F$, waves are generated along the curved wall, producing wavefronts projecting perpendicular to the pillars [12]. The wave fronts from neighboring pillars evidently merge to form the sloshing ridges. These ridges persist even above the regime where self-imaging is observed [see Fig. 2(d)]. We infer that, when a periodic row of pillars is present, laterally sloshing ridges between the pillars act as sources of Faraday waves emitted from between the pillars. In the context of our subsequent theoretical developments it is important to note that it is not the pillars themselves that act as sources of Faraday waves, but rather the sloshing ridges between them.
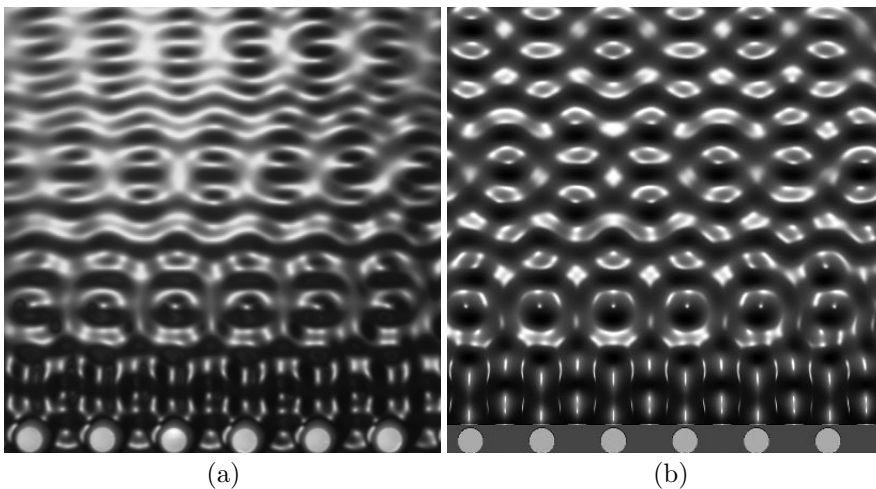
FIG. 4. (a) Observed and (b) computed fluid surface height viewed from directly above, under oblique illumination. Circles at the bottom indicate the location of the pillars. Pillar spacing $d = 9.5$ mm, number of pillars $N = 14$, driving frequency $f = 80$ Hz, Faraday wavelength $\lambda_F = 4.75$ mm, and forcing acceleration $\gamma = 1.007\gamma_F$.

B. Modeling

We model this hydrodynamic Talbot effect in terms of a periodic array of point sources emitting scalar waves. Guided by our observations, we treat the sources as emitters of subharmonic Faraday waves located between the pillars. We define the x axis as lying along the pillars and the y axis transverse to the pillars [see Fig. 1(b)]. The elementary solution to the two-dimensional wave equation is $J_0(kr)e^{-i\omega t}$, where $J_0(kr)$ is the Bessel function of the first kind. When $kr \gg 1$, the Bessel function can be approximated as $J_0(x) \sim \cos(x - \pi/4)/\sqrt{\pi x/2}$. In adding waves from coherent sources, we can suppress the phase $\pi/4$, and so write the displacement of fluid at a position $P(x, y)$ [Fig. 1(b)] as the following superposition:

$$u(x, y, t) = A_F \sum_{n=1}^{N-1} \frac{\cos(k_F r_n - \omega_F t)}{\sqrt{k_F r_n}}, \tag{3}$$

where A_F is the wave amplitude, $r_n = \sqrt{y^2 + (x - (n - 1/2)d)^2}$, $\omega_F = \pi f$, and k_F is the wave number for Faraday waves, prescribed by the standard water-wave dispersion relation, Eq. (1). Using Eq. (3), we compute the displacement $u(x, y, t)$ at each point, nondimensionalized by the wave amplitude A_F. In order to compare the simulation results with experimental videos, we use Surface Plot in MATLAB to visualize the surface elevation. The reflectance properties of the surface are chosen such that the resulting grey scale in our simulations is consistent with that captured in our experiments. Figure 4 shows a side-by-side comparison of the simulated and experimentally observed fluid surface, revealing that the essential features of the observed patterns are adequately captured by Eq. (3).

In our system, the self-images are generated predominantly by the Faraday waves emitted between the pillars. For comparison between our experiments and the classical optics theory, which is for a monochromatic source of wavelength λ, we use the Faraday wavelength in Eq. (2) to evaluate the Faraday-Talbot length,

$$z_F = z_T(\lambda_F) = \frac{\lambda_F}{2\left(1 - \sqrt{1 - \left(\frac{\lambda_F}{d}\right)^2}\right)}. \tag{4}$$
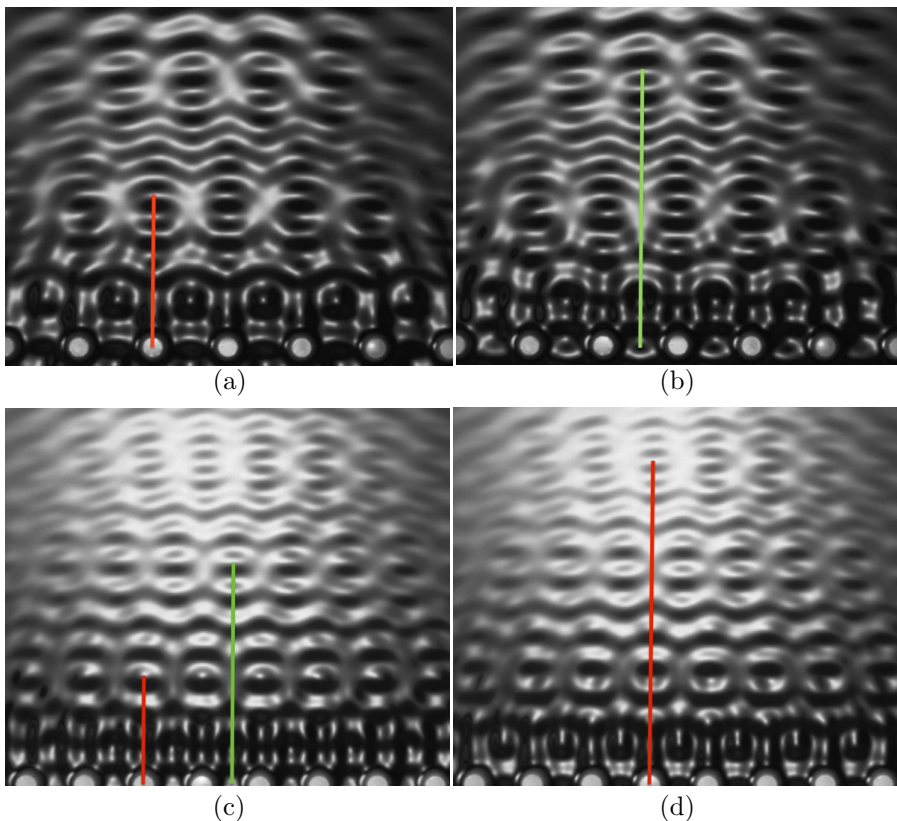
FIG. 5. Self-image locations are evident on video frames half a Faraday period apart. Green lines indicate distances to the in-phase self-images of Faraday wave sources and red lines to the shifted self-images of Faraday wave sources. (a),(b) Array spacing $d = 12.5$ mm, $f = 58$ Hz. Frames (a) and (b) are 1/58 s apart. (c),(d) Array spacing $d = 9.5$ mm, $f = 80$ Hz. Frames (c) and (d) are 1/80 s apart.

Since the sources of Faraday waves are the subharmonic sloshing ridges between the pillars, self-images that are aligned with the pillars occur at odd integer multiples of z_F while those aligned with the gaps are at even integer multiples of z_F. Figure 5 shows the measured distances of the self-images and shifted self-images in the video frames. Self-images further from the pillars are not as sharp, resulting in larger measurement errors.

For both arrays, the measured image locations are in excellent agreement with the calculated Faraday-Talbot length z_F. Figure 6 summarizes the results in a plot of experimental image position versus predicted image position. Note that the image positions are integer multiples of z_F.

C. Trapping of bouncing and walking droplets

We explore the trapping properties of the resulting wave field for bouncing and walking droplets by introducing droplets of silicone oil on the surface of the bath [7]. The dependence of the bouncing and walking behavior on drop size and forcing acceleration has been well characterized both experimentally [8] and theoretically [30]. We generate stationary bouncing droplets by rapidly extracting a pin to break the interface. We then gradually increase the forcing acceleration until the wave field generated by the pillars is formed, and track the drift of the bouncing droplets over time. For self-propelling walking droplets, where control of drop size was required, we utilize a piezoelectric droplet generator to make a single droplet of radius $R = 0.395 \pm 0.005$ mm [31]. We
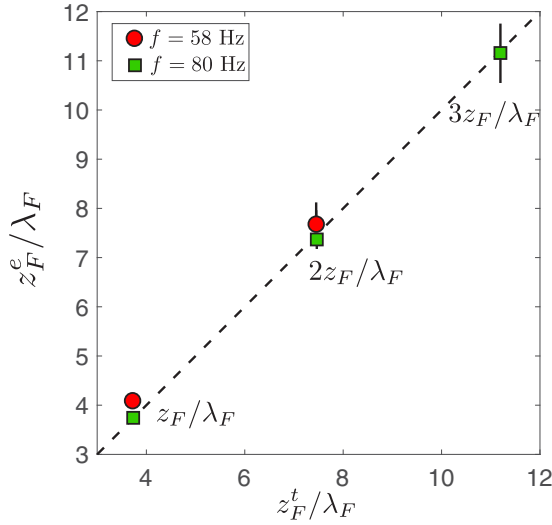
FIG. 6. Plot of the experimentally observed self-image positions (z_F^e) vs predicted self-image positions (z_F^t) for two different forcing frequencies. Lengths are nondimensionalized by the Faraday wavelength λ_F. The predicted self-image positions are at integer multiples of the Faraday-Talbot length z_F, as defined in Eq. (4). Circles: Driving frequency $f = 58$ Hz, $\lambda_F = 6.13$ mm, pillar spacing $d = 12.5$ mm, $z_F = 23.9$ mm. Squares: $f = 80$ Hz, $\lambda_F = 4.75$ mm, $d = 9.5$ mm, $z_F = 17.7$ mm.

then increase the forcing acceleration beyond the Faraday threshold, and direct the walking droplet towards the row of pillars.

In the absence of pillars, static bouncing droplets would bounce in place indefinitely. However, as we gradually increase the forcing acceleration of the bath, enhancing the wave field generated by the pillars, we note that the droplets begin to drift. Once the drifting is complete, bouncing droplets align along rows of images, specifically at distances an integer number of the Faraday-Talbot length away from the row of pillars. The bouncing droplets bounce stably between images, as shown in Fig. 7(a), where the images are denoted by black crosses.

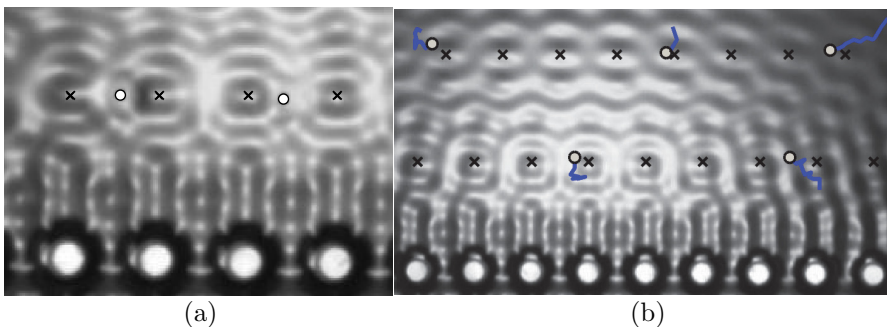(a)   (b)

FIG. 7. Bouncing droplets (small white circles) drift towards the Faraday-Talbot length, and become localized between consecutive pillar images, denoted by black crosses. (a) Two bouncers trapped within the first row of images. This configuration arises for bouncing droplets of different sizes and bouncing modes. (b) Slow drifting motion of bouncing droplets over time: the white circles indicate the final bouncer positions, and the blue trail their trajectories. Bouncers initially close to the pillars tend to drift towards the first row of images, while more distant bouncers are attracted to the second row of images.
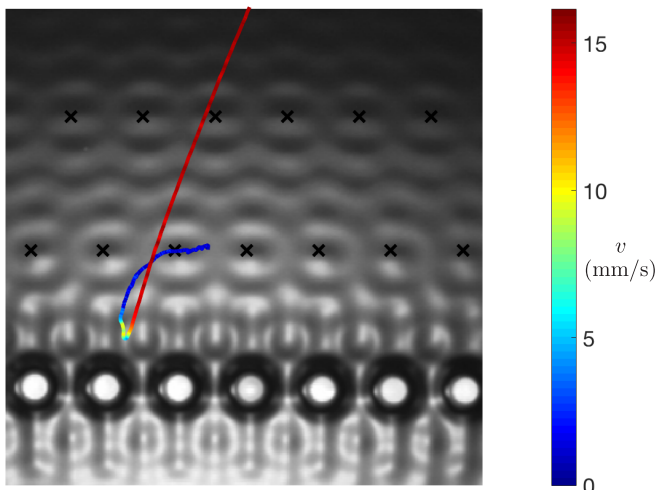
FIG. 8. A walking droplet with radius $R = 0.395 \pm 0.005$ mm impinges on a row of pillars. The droplet approaches with a speed of approximately 16 mm/s before being transformed from a resonant walker to a chaotic bouncer. Thereafter, it slowly drifts towards the first row of Talbot images. The droplet trajectory is color-coded according to speed.

We note that the drift towards the rows of images arises from a wide range of initial bouncing locations. Figure 7(b) illustrates how bouncing droplets that start close to the row of pillars will drift towards the first row of images and settle there. Bouncers initially placed farther away generally drift towards the nearest row of images, which in Fig. 7(b) corresponds to twice the Faraday-Talbot length. The resulting lattice configurations may destabilize in response to drop-drop interactions, when the wave field generated by the other bouncers supersedes the background wave field generated by the pillars.

We also explored the behavior of relatively energetic walking droplets near the Talbot images when the forcing acceleration was above the Faraday threshold, $\gamma \geqslant \gamma_F$. Specifically, we generated droplets of radius $R = 0.395 \pm 0.005$ mm and free walking speed $u_0 \approx 16$ mm/s, and directed them toward the row of pillars. After interacting with the row of pillars, the vertical dynamics of the droplets can change drastically, transforming a fast walker into a chaotic bouncer. This bouncer may then exhibit behavior similar to those in the previous experiments, slowly drifting towards the Faraday-Talbot length, with a tendency to settle between images. A sample trajectory is shown in Fig. 8, emphasizing how the droplet's horizontal speed changes drastically after interacting with the pillar [29].

III. CONCLUSION

We have reported a hydrodynamic analog of the Talbot effect arising on the surface of a vertically shaken fluid with a periodic array of protruding pillars. The effect is observed only for driving frequencies such that the Faraday wavelength is approximately half the pillar spacing and for driving accelerations that are approximately 0.2–1% above the Faraday threshold. The patterns oscillate at half the driving frequency, revealing their sources as sloshing Faraday waves excited between the pillars. A Faraday-Talbot length was defined [Eq. (4)] that rationalizes the locations of the in-phase and shifted out-of-phase self-images.

Video recordings show laterally sloshing fluid ridges between the pillars that act as the Faraday wave sources. There are also quickly decaying meniscus waves emitted from the pillars at the driving frequency that mix with the Faraday waves close to the pillars. While the self-images are

formed from Faraday waves, the presence of meniscus waves adjoining the pillars plays a critical role in seeding the Faraday waves. The importance of the meniscus waves was underscored when we tried the experiment using arrays of submerged pillars (0.3 mm below the fluid surface), and the self-imaging did not arise.

In the optical Talbot effect, the observed light intensity is due to the diffraction and interference of light from an illuminated grating. Although the grating is a passive element, it modulates the light, producing a coherent, periodic source of waves emanating from the grating. In our experiment, sloshing waves generated by the row of pillars serve as the active element. The coherent waves emanating from between the pillars interfere to form the observed Faraday-Talbot pattern. In both cases, the pattern is the result of interference of waves from coherent periodic sources.

The possibility of using the Faraday-Talbot effect for trapping bouncing and walking droplets has been demonstrated, and represents a hydrodynamic analog of particle trapping with the Talbot effect [21,22,32]. Stationary bouncers simply drift towards the images, to be trapped between them. The relatively energetic walkers have their vertical dynamics altered through their interaction with the pillars, resulting in stationary bouncers trapped between the Faraday-Talbot images. Finally, in the broader context of hydrodynamic analogs with the Faraday system [9,33], this represents the first example of an analog of an optical system arising above the Faraday threshold, a parameter regime to be explored further in future studies.

---

[1] I. Newton, *Opticks, Or, A Treatise of the Reflections, Refractions, Inflections & Colours of Light*, Dover Books on Physics (Dover, Mineola, NY, 1952).

[2] T. Young, The Bakerian lecture: Experiments and calculations relative to physical optics, Philos. Trans. R. Soc. London **94**, 1 (1804).

[3] W. G. Unruh, Experimental Black-Hole Evaporation, Phys. Rev. Lett. **46**, 1351 (1981).

[4] G. Jannes, R. Piquet, P. Maïssa, C. Mathis, and G. Rousseaux, Experimental demonstration of the supersonic-subsonic bifurcation in the circular jump: A hydrodynamic white hole, Phys. Rev. E **83**, 056312 (2011).

[5] M. V. Berry, R G Chambers, M. D. Large, C. Upstill, and J. C. Walmsley, Wavefront dislocations in the Aharonov-Bohm effect and its water wave analogue, Eur. J. Phys. **1**, 154 (1980).

[6] B. C. Denardo, J. J. Puda, and A. Larraza, A water wave analog of the Casimir effect, Am. J. Phys. **77**, 1095 (2009).

[7] Y. Couder, S. Protière, E. Fort, and A. Boudaoud, Dynamical phenomena: Walking and orbiting droplets, Nature (London) **437**, 208 (2005).

[8] S. Protière, A. Boudaoud, and Y. Couder, Particle-wave association on a fluid interface, J. Fluid Mech. **554**, 85 (2006).

[9] J. W. M. Bush, Pilot-wave hydrodynamics, Annu. Rev. Fluid Mech. **47**, 269 (2015).

[10] J. W. M. Bush, The new wave of pilot-wave theory, Phys. Today **68**(8), 47 (2015).

[11] M. Faraday, On a peculiar class of acoustical figures, and on certain forms assumed by groups of particles upon vibrating elastic surfaces, Philos. Trans. R. Soc. London **121**, 299 (1831).

[12] S. Douady, Experimental study of the Faraday instability, J. Fluid Mech. **221**, 383 (1990).

[13] T. B. Benjamin and F. Ursell, The stability of the plane free surface of a liquid in vertical periodic motion, Proc. R. Soc. A **225**, 505 (1954).

[14] J. Miles and D. Henderson, Parametrically forced surface waves, Annu. Rev. Fluid Mech. **22**, 143 (1990).

[15] E. Wolf and K. Patorski, *Progress in Optics*, Vol. 27 (North-Holland, Amsterdam, 1989).

[16] H. F. Talbot, Facts relating to optical science. No. IV, Philos. Mag. **9**(56), 401 (1836).

[17] Lord Rayleigh, On copying diffraction-gratings, and on some phenomena connected therewith, Philos. Mag. **11**, 196 (1881).

[18] W. B. Case, M. Tomandl, S. Deachapunya, and M. Arndt, Realization of optical carpets in the Talbot and Talbot-Lau configurations, Opt. Express **17**, 20966 (2009).

[19] J. Wen, Y. Zhang, and M. Xiao, The Talbot effect: Recent advances in classical optics, nonlinear optics, and quantum optics, Adv. Opt. Photon. **5**, 83 (2013).

[20] M. V. Berry and S. Klein, Integer, fractional and fractal Talbot effects, J. Mod. Opt. **43**, 2139 (1996).

[21] R. Newell, J. Sebby, and T. G. Walker, Dense atom clouds in a holographic atom trap, Opt. Lett. **28**, 1266 (2003).

[22] Y. Y. Sun, X.-C. Yuan, L. S. Ong, J. Bu, S. W. Zhu, and R. Liu, Large-scale optical traps on a chip for optical sorting, Appl. Phys. Lett. **90**, 031107 (2007).

[23] M. S. Chapman, C. R. Ekstrom, T. D. Hammond, J. Schmiedmayer, B. E. Tannian, S. Wehinger, and D. E. Pritchard, Near-field imaging of atom diffraction gratings: The atomic Talbot effect, Phys. Rev. A **51**, R14 (1995).

[24] L. Deng, E. W. Hagley, J. Denschlag, J. E. Simsarian, Mark Edwards, Charles W. Clark, K. Helmerson, S. L. Rolston, and W. D. Phillips, Temporal, Matter-Wave-Dispersion Talbot Effect, Phys. Rev. Lett. **83**, 5407 (1999).

[25] W. Zhang, C. Zhao, J. Wang, and J. Zhang, An experimental study of the plasmonic Talbot effect, Opt. Express **17**, 19757 (2009).

[26] T. Weitkamp, A. Diaz, C. David, F. Pfeiffer, M. Stampanoni, P. Cloetens, and E. Ziegler, X-ray phase imaging with a grating interferometer, Opt. Express **13**, 6296 (2005).

[27] D. M. Harris and J. W. M. Bush, Generating uniaxial vibration with an electrodynamic shaker and external air bearing, J. Sound Vib. **334**, 255 (2015).

[28] G. B. Whitham, *Linear and Nonlinear Waves*, Pure and Applied Mathematics: A Wiley Series of Texts, Monographs and Tracts (Wiley, New York, 2011).

[29] See Supplemental Material at http://link.aps.org/supplemental/10.1103/PhysRevFluids.2.103602 for Video 1, showing the oscillating pattern of self-images adjacent to the pillars, and Video 2, showing the trapping of a fast walking drop after interacting with the row of pillars.

[30] J. Moláček and J. W. M. Bush, Drops bouncing on a vibrating bath, J. Fluid Mech. **727**, 582 (2013).

[31] D. M. Harris, T. Liu, and J. W. M. Bush, A low-cost, precise piezoelectric droplet-on-demand generator, Exp. Fluids **56**, 83 (2015).

[32] C. Mennerat-Robilliard, D. Boiron, J. M. Fournier, A. Aradian, P. Horak, and G. Grynberg, Cooling cesium atoms in a Talbot lattice, Europhys. Lett. **44**, 442 (1998).

[33] B. Filoux, M. Hubert, P. Schlagheck, and N. Vandewalle, Walking droplets in linear channels, Phys. Rev. Fluids **2**, 013601 (2017).